Thermal Hall effect in the van der Waals ferromagnet CrI₃

Chunqiang Xu,[1,2,*] Heda Zhang,[1,*] Caitlin Carnahan,[3] Pengpeng Zhang,[1] Di Xiao,[4,5] and Xianglin Ke [1]

[1]*Department of Physics and Astronomy, Michigan State University, East Lansing, Michigan 48824-2320, USA*
[2]*School of Physical Science and Technology, Ningbo University, Ningbo 315211, China*
[3]*Department of Physics, Carnegie Mellon University, Pittsburgh, Pennsylvania 15213, USA*
[4]*Department of Materials Science and Engineering, University of Washington, Seattle, Washington 98195, USA*
[5]*Department of Physics, University of Washington, Seattle, Washington 98195, USA*

CrI₃ is a prototypical van der Waals ferromagnet with a magnetic honeycomb lattice. Previous inelastic neutron scattering studies have suggested topological nature of its magnetic excitations with a magnon gap at the Dirac points, which are anticipated to give rise to magnon thermal Hall effect. Here we report thermal transport properties of CrI₃ and show that the long-sought thermal Hall signal anticipated for topological magnons is fairly small. In contrast, we find that CrI₃ exhibits an appreciable anomalous thermal Hall signal at lower temperature that may arise from magnon-phonon hybridization or magnon-phonon scattering. These findings are anticipated to stimulate further neutron scattering studies on CrI₃ single crystal, which can shed light not only on the intrinsic nature of magnetic excitations but also on the magnon-phonon interaction.

I. INTRODUCTION

The discovery of exotic electronic properties in monolayer graphene has opened a new research arena of searching for novel quasi-two-dimensional (2D) van der Waals (vdW) materials beyond graphene [1,2]. One prominent class of such materials are vdW magnets. With magnetism acting as a control knob, 2D vdW magnets provide an exciting playground for the discovery and exploration of novel physical phenomena and perhaps new physics [3–6]. In addition to various magnetic ground states and unconventional magnetism, vdW magnets also display many other novel phenomena. For instance, ferromagnetism can persist down to the monolayer limit owing to the material's magnetic anisotropy [7,8]. Depending on the layer numbers, the magnetic ground state of exfoliated vdW magnets varies [7]. One can also tune the magnetic ground properties using various nonthermal perturbations, such as strain [9,10], electric gating [11,12], proximity effect [13–16], etc. Furthermore, new phenomena—so-called moiré magnetism—can emerge by stacking layers of vdW magnets on top of each other with certain twisting angles [17–19].

In addition to the interesting static magnetic properties, another intriguing aspect of vdW magnets is due to the potential topological characteristic of their magnetic excitations. Particularly, vdW ferromagnets with magnetic ions occupying a kagome lattice or a honeycomb lattice were proposed to host topological magnons [20,21]. In a ferromagnetic kagome lattice or honeycomb lattice, there are six symmetry-protected magnon band crossings at K points, which retain their degeneracy in the presence of symmetric exchange interactions (e.g., Heisenberg interactions). Because of the inversion symmetry breaking relative to the center of the nearest-neighbor bond of kagome lattice or the second nearest-neighbor bond of honeycomb lattice, the asymmetric Dzyaloshinskii-Moriya interaction (DMI) consequently lifts the degeneracy at these K points and leads to the opening of magnon gaps. By calculating the Berry curvature of these gapped magnon bands and the associated Chern number, it has been shown that the gapped magnon bands are topological in nature [20,21]. Such unique magnon modes can give rise to the thermal Hall effect (THE), i.e., an induced transverse heat flow in the presence of a longitudinal temperature gradient [22,23].

The magnon gap opening at K points and the emergence of the THE have been reported in Cu(1,3-bdc) (bdc = benzenedicarboxylate), which has a kagome lattice of Cu²⁺ ions, suggesting that the magnetic excitations of Cu(1,3-bdc) are topological in nature [24,25]. For a ferromagnetic honeycomb lattice, the most salient system is CrI₃ in which the inelastic neutron scattering (INS) studies have found a gap opening at the K points of magnon bands [26]. However, the underlying mechanism of the observed gap opening remains controversial [26–31]. For instance, is it driven intrinsically by the DMI [26] or the Kitaev interaction [28], or associated with the interlayer couplings [30], or perhaps driven extrinsically by the mosaic of coaligned samples for neutron scattering studies [27]? Surprisingly, to date there is no report of the THE in literature on CrI₃, despite the fact that the magnon THE provides smoking-gun evidence of the topological character of low-energy magnetic excitations.

In this work, we report the thermal transport studies of CrI₃ single crystals. We find that the thermal Hall signal associated with the anticipated topological magnetic excitations is fairly small, about an order in magnitude smaller than the predicted value based on the reported DMI values

---

*These authors contributed equally to this work.

in previous INS studies [26,27]. In contrast, we show that CrI_3 exhibits an appreciable anomalous thermal Hall signal at low temperature, which is presumably of phononic origin. Potential mechanisms of the THE features observed in CrI_3 are discussed.

II. EXPERIMETNAL METHODS

CrI_3 has a layered structure with a honeycomb layer of chromium atoms separated by two layers of iodine atoms along the c axis, as shown in Fig. S1 in the Supplemental Material [32]. It undergoes a paramagnetic-to-ferromagnetic phase transition with $T_c \sim 60$ K and spins aligned along the c axis [33]. In this work, single crystals of CrI_3 were synthesized using the chemical vapor transport method [33]. The magnetic susceptibility data were measured using a superconducting quantum interference device (Quantum Design). The thermal transport measurements were conducted using a one-heater three-sensor technique on a sample puck adapted to a physical property measurement system (Quantum Design). The longitudinal and transverse thermal conductivity were simultaneously measured using a conventional steady-state method. The magnetic field was applied along the magnetic easy axis, i.e., c axis. A schematic of the experimental setup for thermal transport measurements is shown in Fig. S2 [32], and more detailed information can be found in the Supplemental Material of Ref. [34]. To minimize exposing the CrI_3 samples to the air (moisture), the devices were prepared inside a glove bag equipped with an internal microscope and a continuous flow of high-purity nitrogen gas.

III. RESULTS AND DISCUSSION

Figure 1(a) shows the temperature dependence of magnetic susceptibility (χ_c) of CrI_3 measured under zero-field-cooled (ZFC) condition with an applied field of 0.1 T ($\mu_0 \vec{H} \parallel \vec{c}$). χ_c sharply increases below the ordering temperature T_c of $\sim$60 K and then saturates, indicative of a ferromagnetic phase transition, which is consistent with the literature [33]. In Fig. 1(b), we present the thermal conductivity (κ_{xx}) measured as a function of temperature at 0 and 5 T magnetic field ($\mu_0 \vec{H} \parallel \vec{c}$). There are a couple of noteworthy features. First, no anomaly in κ_{xx} is obviously observed near T_c. Since CrI_3 is an insulator, its total κ_{xx} is composed of magnon (κ^{mag}) and phonon (κ^{ph}) contributions. Thus, the little effect of magnetic ordering on κ_{xx} suggests that κ^{ph} dominates over κ^{mag} in CrI_3, a feature distinct from its sister compound $CrCl_3$ [35]. Second, the change in κ_{xx} induced by an applied magnetic field ($\Delta\kappa_{xx} = \kappa_{xx}^{5\,T} - \kappa_{xx}^{0\,T}$) is very subtle compared to the signal itself. Therefore, to better quantify this change, we plot $\Delta\kappa_{xx}$ as a function of temperature in Fig. 1(c) together with the scaled temperature derivative of $\frac{1}{\chi_c}|\frac{d\chi_c}{dT}|$ for reference. We can see that both curves exhibit an upward trend above T_c, which is due to the onset of short-range magnetic correlations prior to the long-range order. The positive value of $\Delta\kappa_{xx}$ in the high-temperature regime indicates the existence of magnon-phonon coupling in CrI_3. While magnons and phonons contribute individually to the thermal conduction, they also scatter each other, which tends to suppress the total thermal conduction. At high temperatures, in the absence of
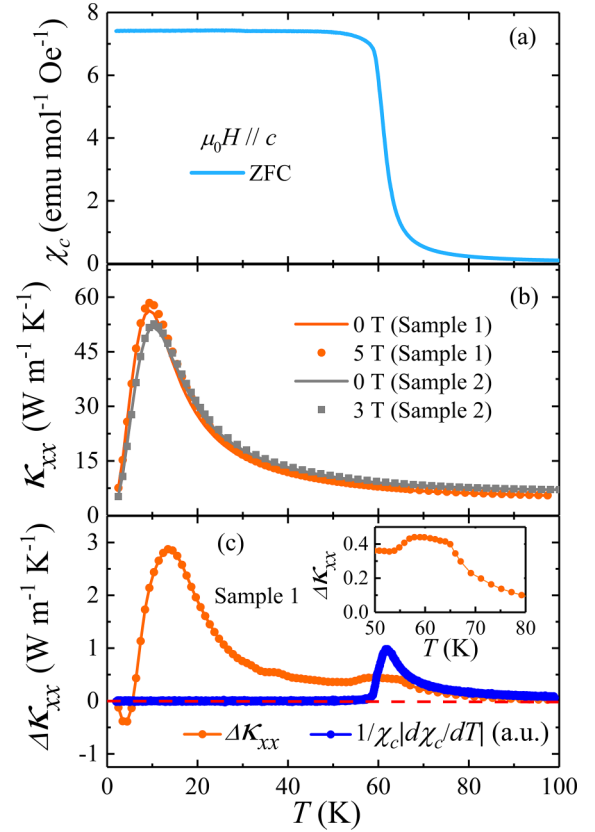

FIG. 1. (a) The temperature dependence of magnetic susceptibility (χ_c) measured at 0.1 T under zero-field-cooled (ZFC) condition. (b) The temperature dependence of κ_{xx} of two samples measured at 0 T and high magnetic fields. (c) Temperature vs $\Delta\kappa_{xx}$ ($\Delta\kappa_{xx} = \kappa_{xx}|_{5\,T} - \kappa_{xx}|_{0\,T}$) (black) and temperature derivative of magnetic susceptibility $\frac{1}{\chi_c}|\frac{d\chi_c}{dT}|$ (red).

magnetic field magnons (or incoherent magnons right above T_c) scatter phonons, which reduces the κ^{ph} contribution and dominates over the κ^{mag} term. An applied magnetic field suppresses magnon population by lifting the magnon bands to higher energy, which subsequently reduces the phonon scattering by magnons and (partially) restores the κ^{ph} contribution and thus enhances the total κ_{xx}, leading to positive $\Delta\kappa_{xx}$. A similar feature has been observed in another CrI_3 sample as shown in Fig. 1 and in Fig. S3 [32] and in other vdW magnets, such as $CrCl_3$ [35], VI_3 [34], and $FeCl_2$ [36]. $\Delta\kappa_{xx}$ changes the sign below 6 K, implying that in the lower-temperature region the field-induced reduction of magnon contributions to κ_{xx} is larger than the restoration of phonon contribution due to the suppression of phonon scattering by magnons. Note that while the low-temperature κ_{xx} value of CrI_3 is nearly an order of magnitude larger than that of VI_3 (Fig. S4), $\Delta\kappa_{xx}/\kappa_{xx}$ is comparable, which implies a similar strength of magnon-phonon coupling in both compounds.

We move on to discuss the transverse thermal signal of CrI_3. As will be shown later, it is worth noting that the magnitude of the intrinsic thermal Hall resistivity $|w_{yx}|$ of CrI_3 (in the order of 10^{-5} K m W^{-1}) is found to be much smaller than that of the longitudinal thermal resistivity w_{xx}. Therefore, when dealing with signals with such small
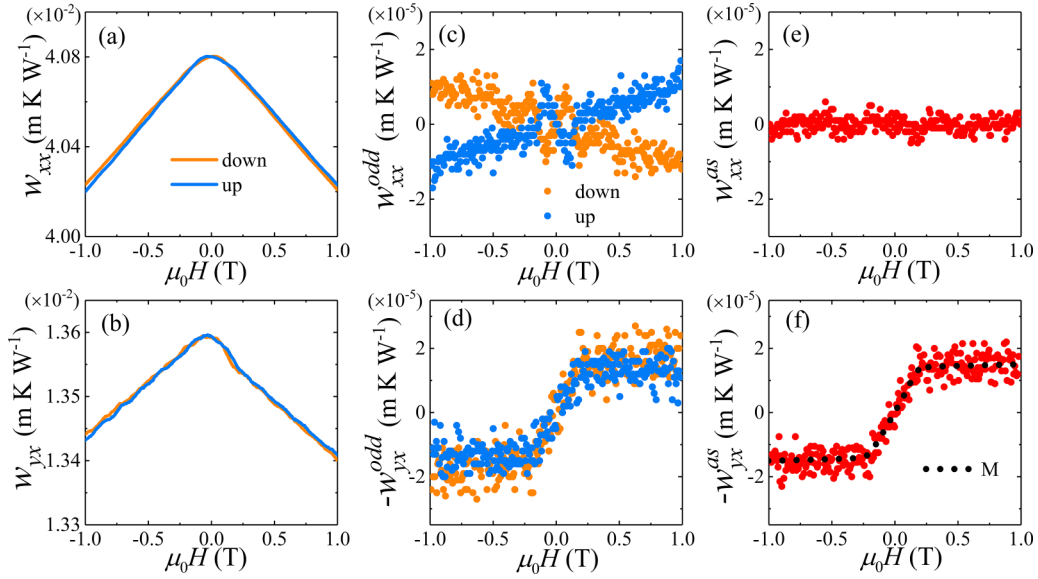
FIG. 2. (a) Thermal resistivity w_{xx} hysteresis between -1 and 1 T. (b) Thermal Hall resistivity w_{yx} hysteresis between -1 and 1 T. (c), (d) The odd component w_{xx}^{odd} and $-w_{yx}^{odd}$ [$w^{odd} = (w^{H+} - w^{H-})/2$], which are from (a) and (b). (e), (f) Asymmetric component w_{xx}^{as} and $-w_{yx}^{as}$ [$w^{as} = (w^{odd,up} + w^{odd,down})/2$], which are from (c) and (d); the dashed black line is magnetization curve $M(H)$. Data were measured at $T = 23.7$ K.

magnitude, validating the intrinsic nature of the observed signal is pressing [37]. Here, we examine the nature of the THE observed in CrI$_3$ by studying the hysteresis behavior, the applied heating power dependence, and the sample dependence. We first present the hysteresis behavior of both longitudinal and transverse thermal resistivity and demonstrate that these two measured quantities exhibit distinct behaviors. In Figs. 2(a) and 2(b), we present the raw measurement data of w_{xx} and w_{yx} measured at $T = 23.7$ K. Here the orange and blue curves represent the data measured during field ramping down (1 to -1 T) and ramping up (-1 to 1 T) processes, respectively. In contrast to the measured w_{xx}, which is nearly symmetric between positive and negative fields [Fig. 2(a)], we can see that w_{yx} shows an asymmetry between positive and negative fields that is superimposed with a large symmetric (even) component. Such an even component stems from the w_{xx} contribution introduced due to a small misalignment between the transverse temperature leads, since the intrinsic $|w_{yx}|$ is much smaller than w_{xx}. Generally, one performs antisymmetrization to eliminate the longitudinal contribution to the measured w_{yx}. In Figs. 2(c) and 2(d) we present the odd component [$w^{odd} = (w^{H+} - w^{H-})/2$] of both longitudinal and transverse thermal resistivity as w_{xx}^{odd} and $-w_{yx}^{odd}$, where w^{H+} (w^{H-}) stands for the thermal resistivity measured in the positive (negative) field region. One can see that while the w_{yx}^{odd} data obtained for these two processes are similar to each other, w_{xx}^{odd} shows an opposite trend for two field ramping processes, which arises from the hysteresis of w_{xx}. This suggests that a small misalignment between the transverse temperature leads can cause w_{yx}^{odd} to pick up an extrinsic contribution from w_{xx}^{odd} that cannot be eliminated by simply antisymmetrizing the raw w_{yx} data. Instead, this extrinsic contribution w_{yx}^{odd} can be properly eliminated by averaging the w^{odd} data extracted from both field ramping processes. The resultant asymmetric components [$w^{as} = (w^{odd,up} + w^{odd,down})/2$] for the longitu-

dinal and transverse thermal signal are shown in Figs. 2(e) and 2(f). We can see that w_{xx}^{as} shown in Fig. 2(e) is nearly zero. In contrast, the thus-extracted w_{yx}^{as}, the red symbols shown in Fig. 2(f), shows an odd function of magnetic field whose general shape is similar to the magnetization curve (black dashed line) measured at the same temperature, representing an intrinsic transverse thermal Hall signal. Similar data processing procedures have been previously applied to extract the intrinsic thermal Hall signal in other systems, such as α-RuCl$_3$ [37] and FeCl$_2$ [36].

We also study the dependence of w_{yx}^{as} on the heating power P. For an intrinsic THE, the transverse temperature difference ΔT_{yx} scales linearly with P, as implied from the definition of w_{yx} ($w_{yx} = \frac{\Delta T_{yx}}{P} t$) where t is the thickness of the sample. As shown in Fig. S5, at three different applied heating powers (800, 1000, and 1470 μW), the w_{yx}^{as} signal is nearly identical, indicating that the thermal Hall signal is indeed independent of P. We have also reproduced similar results on another piece of CrI$_3$ sample (see Fig. S6). These results affirm the intrinsic nature of the THE observed in CrI$_3$.

Figure 3 presents the magnetic field dependence of thermal Hall conductivity (κ_{yx}), which is defined as ($\kappa_{yx} = \frac{-w_{yx}^{as}}{w_{xx}^2 + w_{yx}^{as\,2}}$), measured at various temperatures. The dashed curves are guides to the eyes. At low field κ_{yx} increases sharply alike
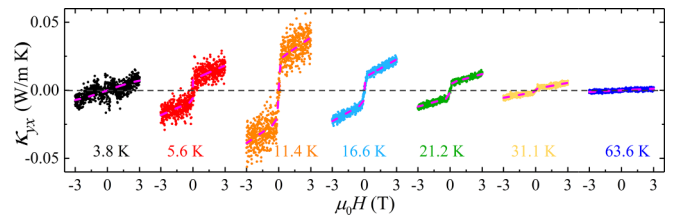

FIG. 3. The thermal Hall conductivity κ_{yx} measured at various temperatures.
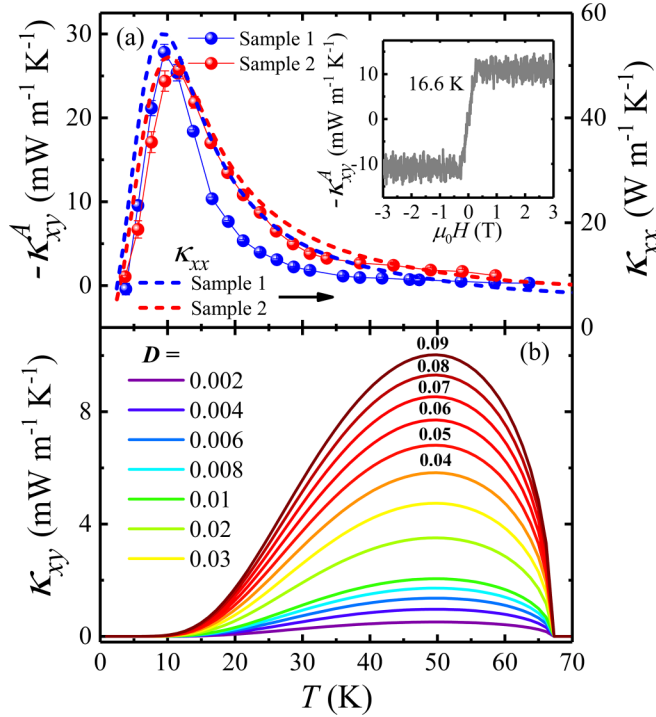
FIG. 4. (a) Temperature dependence of anomalous thermal Hall conductivity $-\kappa_{xy}^{A}$. The $\kappa_{xx}(T)$ curves are overplotted for reference. Inset shows the extracted $-\kappa_{xy}^{A}$ as a function of field at 16.6 K. (b) The calculated κ_{xy} with various DMI values (D).

the $M(H)$ curve seen in Fig. 2(f), suggesting that at low field κ_{yx} mainly arises from the anomalous THE. Upon increasing the magnetic field, there is an additional κ_{yx} component that is linearly proportional to the magnetic field. As shown in Fig. S7, the temperature dependence of the coefficient of this linear THE component displays a broad peak near the same temperature as in the $\kappa_{xx}(T)$ curve. These features are similar to those observed in paramagnetic SrTiO$_3$ [38] or antiferromagnetic Cu$_3$TeO$_6$ [39], implying that this linear THE component is purely driven phonons the mechanism of which is beyond the scope of the current study.

We now focus on the anomalous THE component. To better quantify the temperature dependence of the anomalous thermal Hall signal, Fig. 4(a) shows the temperature dependence of the extracted anomalous thermal Hall conductivity κ_{yx}^{A} ($-\kappa_{xy}^{A}$). There are two features worth pointing out. First, κ_{yx}^{A} exhibits a broad peak around 10 K, which is close to the temperature at which the longitudinal thermal conductivity κ_{xx} maximizes. Similar $\kappa_{yx}^{A}(T)$ behavior is also observed on another sample (Sample 2) shown in Fig. 4(a), affirming its reproducibility. This suggests that the observed κ_{yx}^{A} in this temperature region is related to phonons. However, here κ_{yx}^{A} could not be purely driven by phonons, as evidenced by the extracted $\kappa_{yx}^{A}(H)$ shown in the inset of Fig. 4(a), which resembles the $M(H)$ curve shown in Fig. 2(f). Instead, phonons are responsible for the anomalous THE component κ_{yx}^{A} via magnon(spin)-phonon coupling due to the magnetoelastic interaction. Similar features have been observed in the VI$_3$ system [34]. A plausible mechanism is associated with magnon-phonon hybridization. Magnons and phonons

hybridize at the band anticrossing points, forming a new type of quasiparticle, the magnon-polaron. Berry curvature hotspots are induced in the region near the anticrossing points between the two hybridized bands, which are anticipated to give rise to a THE [40–43]. Recent first-principles calculations showed that, without considering the spin-lattice coupling, the low-energy magnon bands and the acoustic phonon bands cross each other at ~1.5 and 5.0 meV, at which an observation of the hybridization gap is anticipated when spin-lattice coupling is taken into account [31]. A future INS study to directly probe potential magnon-phonon hybridizations in CrI$_3$ is desirable. Another plausible mechanism to explain the anomalous THE component is magnon-phonon scattering. As discussed previously, phonons are scattered by magnons, which results in slight suppression of κ_{xx}. It was recently predicted that, similar to the extrinsic anomalous Hall effect induced by skew scattering and side-jump scattering of charge carriers, scattering of phonons by collective fluctuations may give rise to the THE [44].

Second, the κ_{yx}^{A} value drops quickly to nearly zero in the high-temperature region. This finding is a surprise and it is in sharp contrast to the $\kappa_{yx}^{A}(T)$ observed in VI$_3$ in which a large thermal Hall signal is observed over a wide range of temperature nearly up to T_c [34]. As discussed in the Introduction, the sizable magnon gap at K points observed in CrI$_3$ via INS studies, which was ascribed to the DMI [26,27], suggests the topological nature of magnetic excitations in CrI$_3$ that is anticipated to lead to the THE. To support this, we have simulated the magnon bands using a Hamiltonian consisting of exchange parameters extracted from the most recent INS studies [27] and calculated the corresponding thermal Hall conductivity. As shown in Fig. 4(b), with a DMI of 0.09 meV that was recently reported [27], an appreciable thermal Hall signal is anticipated in the high-temperature region with a maximum value of ~0.01 W m^{-1} K^{-1}, which is nearly an order of magnitude larger than the experimental observation presented in Fig. 4(a). This raises an intriguing question: Why is the observed thermal Hall signal in CrI$_3$ so small in the high-temperature region compared to the theoretical prediction?

One possible scenario is that the DMI value extracted by fitting the magnetic excitations obtained based on the INS studies using the linear spin wave theory might be overestimated. Indeed, a recent INS study found that the mosaic of coaligned CrI$_3$ single crystals artificially contributes to the magnons gap opening at K points, which can lead to an overestimation of the DMI value [26,27]. This is also strongly supported by recent INS studies on a single, large piece of single crystal of CrBr$_3$ [45] and CrCl$_3$ [46] in which the magnon bands cross each other at K points within the instrumental energy resolution, which is in contrast to the observation of a large magnon gap reported in coaligned CrBr$_3$ single crystals [47]. These results suggest that the intrinsic DMI is neglectable in both CrBr$_3$ and CrCl$_3$ [45,46]. Although the spin-orbit coupling of iodine atoms is larger than that of bromine and chlorine atoms, which may lead to a larger DMI in CrI$_3$ than that of CrBr$_3$ and CrCl$_3$, it is likely that the previously determined DMI in CrI$_3$ based on the most recent INS studies is still overestimated due to the 8° sample mosaic

of the coaligned single crystals (compared to 17° reported in an earlier study) [26,27]. In Fig. 4, we plot the calculated thermal Hall conductivity based on a 2D monolayer model with various DMI values. We can see that the calculated thermal Hall conductivity with a DMI of 0.01 meV better agrees with the experimental data.

Another possible mechanism to account for the small thermal Hall signal may be ascribed to the combined effects of the interlayer coupling and the third-neighbor intralayer interaction in CrI_3. Note that the sign of κ_{xy}^A in CrI_3 is opposite to that found in VI_3 [34]. Recent theoretical calculations showed that the thermal Hall conductivity in CrI_3 strongly depends on both the interlayer coupling and the third-neighbor intralayer coupling J_3 and that even the sign of κ_{xy} can change [29]. With certain phase parameters, the magnetic excitation becomes gapless Weyl type instead of a topological magnon insulator, which gives rise to a zero/small thermal Hall signal [29]. INS studies on a large, single piece of CrI_3 single crystal are demanding, which may allow further determination of the exchange interactions and DMI without the need to consider the extrinsic effect stemming from the mosaic of coaligned samples. This will help to clarify the topological nature of magnetic excitations in CrI_3 and to clarify the mechanisms that account for the thermal Hall signal observed in this study.

Finally, we would like to briefly comment on the potential effects of magnon-magnon interactions on κ_{xx}. Due to the absence of particle-number conservation law for bosonic excitations, the magnon-magnon interactions can affect the topology of magnetic excitations and thus affect the THE. On the one hand, magnon-magnon interactions can give rise to magnon damping, which is anticipated to suppress κ_{xy} [48]. However, magnon damping in CrI_3 was not discernible in the previous INS studies [26,27]. It is likely that the higher-order magnon-magnon interactions need to be taken into account for the suppression of κ_{xy}, as argued in a recent study of $SrCu_2(BO_3)_2$ [49]. On the other hand, a recent theoretical study suggested that, instead of being detrimental to topology,

magnon-magnon interactions can serve as a source of topology of magnon bands and lead to the THE [50].

IV. CONCLUSION

In summary, we report thermal transport properties of the 2D vdW honeycomb ferromagnet CrI_3, a long-sought topological magnon insulator candidate. We show that the thermal Hall signal in the higher temperature region, which is anticipated for topological magnon insulators, is fairly small. An intrinsically small DMI or the cooperative effect of interlayer coupling and intralayer interaction may account for this observation. In contrast, we find that CrI_3 exhibits THE with an appreciable anomalous thermal Hall signal in the lower-temperature region, which may arise from magnon-phonon hybridization or magnon-phonon scattering. These findings will stimulate future INS studies on a large, single piece of CrI_3 crystal, which can shed light not only on the magnon-phonon interaction but also on the intrinsic nature of magnetic excitations, which will in turn help elucidate the observed THE phenomena in this study.

Data for the figures presented in this paper are available at Ref. [51].

[1] G. R. Bhimanapati *et al.*, Recent advances in two-dimensional materials beyond graphene, ACS Nano **9**, 11509 (2015).

[2] A. Gupta, T. Sakthivel, and S. Seal, Recent development in 2D materials beyond graphene, Prog. Mater. Sci. **73**, 44 (2015).

[3] J.-G. Park, Opportunities and challenges of 2D magnetic van der Waals materials: Magnetic graphene? J. Phys.: Condens. Matter **28**, 301001, (2016).

[4] N. Samarth, Magnetism in flatland, Nature (London) **546**, 216 (2017).

[5] K. S. Burch, D. Mandrus, and J.-G. Park, Magnetism in two-dimensional van der Waals materials, Nature (London) **563**, 47 (2018).

[6] M. Blei, J. L. Lado, Q. Song, D. Dey, O. Erten, V. Pardo, R. Comin, S. Tongay, and A. S. Botana, Synthesis, engineering, and theory of 2D van der Waals magnets, Appl. Phys. Rev. **8**, 021301 (2021).

[7] B. Huang, G. Clark, E. Navarro-Moratalla, D. R. Klein, R. Cheng, K. L. Seyler, D. Zhong, E. Schmidgall, M. A. McGuire, D. H. Cobden, W. Yao, D. Xiao, P. Jarillo-Herrero, and X.

Xu, Layer-dependent ferromagnetism in a van der Waals crystal down to the monolayer limit, Nature (London) **546**, 270 (2017).

[8] C. Gong, L. Li, Z. Li, H. Ji, A. Stern, Y. Xia, T. Cao, W. Bao, C. Wang, Y. Wang, Z. Q. Qiu, R. J. Cava, S. G. Louie, J. Xia, and X. Zhang, Discovery of intrinsic ferromagnetism in two-dimensional van der Waals crystals, Nature (London) **546**, 265 (2017).

[9] J. Cenker, S. Sivakumar, K. Xie, A. Miller, P. Thijssen, Z. Liu, A. Dismukes, J. Fonseca, E. Anderson, X. Zhu, X. Roy, D. Xiao, J.-H. Chu, T. Cao, and X. Xu, Reversible strain-induced magnetic phase transition in a van der Waals magnet, Nat. Nanotechnol. **17**, 256 (2022).

[10] Y. Wang, C. Wang, S.-J. Liang, Z. Ma, K. Xu, X. Liu, L. Zhang, A. S. Admasu, S.-W. Cheong, L. Wang, M. Chen, Z. Liu, B. Cheng, W. Ji, and F. Miao, Strain-sensitive magnetization reversal of a van der Waals magnet, Adv. Mater. **32**, 2004533, (2020).

[11] S. Jiang, L. Li, Z. Wang, K. F. Mak, and J. Shan, Controlling magnetism in 2D CrI_3 by electrostatic doping, Nat. Nanotechnol. **13**, 549 (2018).

[12] B. Huang, G. Clark, D. R. Klein, D. MacNeill, E. Navarro-Moratalla, K. L. Seyler, N. Wilson, M. A. McGuire, D. H. Cobden, D. Xiao, W. Yao, P. Jarillo-Herrero, and X. Xu, Electrical control of 2D magnetism in bilayer CrI_3, Nat. Nanotechnol. **13**, 544 (2018).

[13] D. Zhong, K. L. Seyler, X. Linpeng, N. P. Wilson, T. Taniguchi, K. Watanabe, M. A. McGuire, K.-M. C. Fu, D. Xiao, W. Yao, and X. Xu, Layer-resolved magnetic proximity effect in van der Waals heterostructures, Nat. Nanotechnol. **15**, 187 (2020).

[14] M. Bora and P. Deb, Magnetic proximity effect in two-dimensional van der Waals heterostructure, JPhys Mater. **4**, 034014, (2021).

[15] C. Gong and X. Zhang, Two-dimensional magnetic crystals and emergent heterostructure devices, Science **363**, eaav4450 (2019).

[16] M. Gibertini, M. Koperski, A. F. Morpurgo, and K. S. Novoselov, Magnetic 2D materials and heterostructures, Nat. Nanotechnol. **14**, 408 (2019).

[17] K. Hejazi, Z.-X. Luo, and L. Balents, Noncollinear phases in moiré magnets, Proc. Natl. Acad. Sci. USA **117**, 10721 (2020).

[18] A. O. Fumega and J. L. Lado, Moiré-driven multiferroic order in twisted $CrCl_3$, $CrBr_3$ and CrI_3 bilayers, 2D Mater. **10**, 025026 (2023).

[19] T. Song, Q.-C. Sun, E. Anderson, C. Wang, J. Qian, T. Taniguchi, K. Watanabe, M. A. McGuire, R. Stöhr, D. Xiao, T. Cao, J. Wrachtrup, and X. Xu, Direct visualization of magnetic domains and moiré magnetism in twisted 2D magnets, Science **374**, 1140 (2021).

[20] S. A. Owerre, A first theoretical realization of honeycomb topological magnon insulator, J. Phys.: Condens. Matter **28**, 386001 (2016).

[21] L. Zhang, J. Ren, J.-S. Wang, and B. Li, Topological magnon insulator in insulating ferromagnet, Phys. Rev. B **87**, 144101 (2013).

[22] A. Mook, J. Henk, and I. Mertig, Magnon Hall effect and topology in kagome lattices: A theoretical investigation, Phys. Rev. B **89**, 134409 (2014).

[23] S. A. Owerre, Topological honeycomb magnon Hall effect: A calculation of thermal Hall conductivity of magnetic spin excitations, J. Appl. Phys. **120**, 043903 (2016).

[24] R. Chisnell, J. S. Helton, D. E. Freedman, D. K. Singh, R. I. Bewley, D. G. Nocera, and Y. S. Lee, Topological magnon bands in a Kagome lattice ferromagnet, Phys. Rev. Lett. **115**, 147201 (2015).

[25] M. Hirschberger, R. Chisnell, Y. S. Lee, and N. P. Ong, Thermal Hall effect of spin excitations in a Kagome magnet, Phys. Rev. Lett. **115**, 106603 (2015).

[26] L. Chen, J.-H. Chung, B. Gao, T. Chen, M. B. Stone, A. I. Kolesnikov, Q. Huang, and P. Dai, Topological spin excitations in honeycomb ferromagnet CrI_3, Phys. Rev. X **8**, 041028 (2018).

[27] L. Chen, J.-H. Chung, M. B. Stone, A. I. Kolesnikov, B. Winn, V. O. Garlea, D. L. Abernathy, B. Gao, M. Augustin, E. J. G. Santos, and P. Dai, Magnetic field effect on topological spin excitations in CrI_3, Phys. Rev. X **11**, 031047 (2021).

[28] I. Lee, F. G. Utermohlen, D. Weber, K. Hwang, C. Zhang, J. van Tol, J. E. Goldberger, N. Trivedi, and P. C. Hammel,

Fundamental spin interactions underlying the magnetic anisotropy in the Kitaev ferromagnet CrI_3, Phys. Rev. Lett. **124**, 017201 (2020).

[29] S. Li and A. H. Nevidomskyy, Topological Weyl magnons and thermal Hall effect in layered honeycomb ferromagnets, Phys. Rev. B **104**, 104419 (2021).

[30] T. Gorni, O. Baseggio, P. Delugas, I. Timrov, and S. Baroni, First-principles study of the gap in the spin excitation spectrum of the CrI_3 honeycomb ferromagnet, Phys. Rev. B **107**, L220410 (2023).

[31] P. Delugas, O. Baseggio, I. Timrov, S. Baroni, and T. Gorni, Magnon-phonon interactions enhance the gap at the Dirac point in the spin-wave spectra of CrI_3 two-dimensional magnets, Phys. Rev. B **107**, 214452 (2023).

[32] See Supplemental Material at http://link.aps.org/supplemental/10.1103/PhysRevB.109.094415 for detailed information of crystal and spin structure, experimental setup, and additional data of thermal transport measurements.

[33] M. A. McGuire, H. Dixit, V. R. Cooper, and B. C. Sales, Coupling of crystal structure and magnetism in the layered, ferromagnetic insulator CrI_3, Chem. Mater. **27**, 612 (2015).

[34] H. Zhang, C. Xu, C. Carnahan, M. Sretenovic, N. Suri, D. Xiao, and X. Ke, Anomalous thermal Hall effect in an insulating van der Waals magnet, Phys. Rev. Lett. **127**, 247202 (2021).

[35] C. A. Pocs, I. A. Leahy, H. Zheng, G. Cao, E.-S. Choi, S. H. Do, K.-Y. Choi, B. Normand, and M. Lee, Giant thermal magnetoconductivity in $CrCl_3$ and a general model for spin-phonon scattering, Phys. Rev. Res. **2**, 013059 (2020).

[36] C. Xu, C. Carnahan, H. Zhang, M. Sretenovic, P. Zhang, D. Xiao, and X. Ke, Thermal Hall effect in a van der Waals triangular magnet $FeCl_2$, Phys. Rev. B **107**, L060404 (2023).

[37] P. Czajka, T. Gao, M. Hirschberger, P. Lampen-Kelley, A. Banerjee, J. Yan, D. G. Mandrus, S. E. Nagler, and N. P. Ong, Oscillations of the thermal conductivity in the spin-liquid state of α-$RuCl_3$, Nat. Phys. **17**, 915 (2021).

[38] X. Li, B. Fauqué, Z. Zhu, and K. Behnia, Phonon thermal Hall effect in strontium titanate, Phys. Rev. Lett. **124**, 105901 (2020).

[39] L. Chen, M.-E. Boulanger, Z.-C. Wang, F. Tafti, and L. Taillefer, Large phonon thermal Hall conductivity in the antiferromagnetic insulator Cu_3TeO_6, Proc. Natl. Acad. Sci. USA **119**, e2208016119 (2022).

[40] R. Takahashi and N. Nagaosa, Berry curvature in magnon-phonon hybrid systems, Phys. Rev. Lett. **117**, 217205 (2016).

[41] G. Go, S. K. Kim, and K.-J. Lee, Topological magnon-phonon hybrid excitations in two-dimensional ferromagnets with tunable Chern numbers, Phys. Rev. Lett. **123**, 237207 (2019).

[42] X. Zhang, Y. Zhang, S. Okamoto, and D. Xiao, Thermal Hall effect induced by magnon-phonon interactions, Phys. Rev. Lett. **123**, 167202 (2019).

[43] S. Park and B.-J. Yang, Topological magnetoelastic excitations in noncollinear antiferromagnets, Phys. Rev. B **99**, 174435 (2019).

[44] L. Mangeolle, L. Balents, and L. Savary, Phonon thermal Hall conductivity from scattering with collective fluctuations, Phys. Rev. X **12**, 041031 (2022).

[45] S. E. Nikitin, B. Fåk, K. W. Krämer, T. Fennell, B. Normand, A. M. Läuchli, and C. Rüegg, Thermal evolution of Dirac

magnons in the honeycomb ferromagnet CrBr$_3$, Phys. Rev. Lett. **129**, 127201 (2022).

[46] S.-H. Do, J. A. M. Paddison, G. Sala, T. J. Williams, K. Kaneko, K. Kuwahara, A. F. May, J. Yan, M. A. McGuire, M. B. Stone, M. D. Lumsden, and A. D. Christianson, Gaps in topological magnon spectra: Intrinsic versus extrinsic effects, Phys. Rev. B **106**, L060408 (2022).

[47] Z. Cai, S. Bao, Z.-L. Gu, Y.-P. Gao, Z. Ma, Y. Shangguan, W. Si, Z.-Y. Dong, W. Wang, Y. Wu, D. Lin, J. Wang, K. Ran, S. Li, D. Adroja, X. Xi, S.-L. Yu, X. Wu, J.-X. Li, and J. Wen, Topological magnon insulator spin excitations in the two-dimensional ferromagnet CrBr$_3$, Phys. Rev. B **104**, L020402 (2021).

[48] A. L. Chernyshev and P. A. Maksimov, Damped topological magnons in the kagome-lattice ferromagnets, Phys. Rev. Lett. **117**, 187203 (2016).

[49] S. Suetsugu, T. Yokoi, K. Totsuka, T. Ono, I. Tanaka, S. Kasahara, Y. Kasahara, Z. Chengchao, H. Kageyama, and Y. Matsuda, Intrinsic suppression of the topological thermal Hall effect in an exactly solvable quantum magnet, Phys. Rev. B **105**, 024415 (2022).

[50] A. Mook, K. Plekhanov, J. Klinovaja, and D. Loss, Interaction-stabilized topological magnon insulator in ferromagnets, Phys. Rev. X **11**, 021061 (2021).

[51] https://doi.org/10.5281/zenodo.10778232.